Journal of Thermal Analysis and Calorimetry (2023) 148:3019–3033
https://doi.org/10.1007/s10973-022-11356-x

A single-step chemistry mechanism for biogas supersonic combustion velocity with nitrogen dilution

Mohammad Nurizat Rahman[1,2] · Mohd Haffis Ujir[2] · Mazlan Abdul Wahid[1] · Mohd Fairus Mohd Yasin[1]

Received: 6 January 2022 / Accepted: 31 March 2022 / Published online: 5 May 2022

Abstract

The application of one-step irreversible Arrhenius kinetics to the numerical description of biogas supersonic combustion (also known as detonation) with nitrogen N_2 dilution is investigated in this study. The three model parameters: the temperature exponent n, the activation energy E_a, and the pre-exponential factor A_r are chosen to describe biogas detonation velocities. It can be seen that as the N_2 dilution reached 50%, changes in E_a caused a significant drop in biogas detonation velocity, which was also observed in the current biogas detonation experiment, demonstrating that the dependence of high and low E_a values could appropriately tailor for changes in the thermodynamic condition of the reaction zone behind the detonation fronts as the N_2 dilution increased. Via the validation feedback loop processes with the experimental and detailed chemistry (GRI Mech 3.0) results as the main validation basis, the resulting chemistry description in the one-step model is able to reproduce biogas detonation velocities with reasonable accuracy (< 15% discrepancy). Hence, the model overcomes the known gap of prior establishments of one-step Arrhenius kinetics for detonation by incorporating the N_2 dilution effect and biogas as a fuel for detonation emergence.

Keywords One-step chemistry · Biogas · Detonation · Dilution · Chemical kinetics

Abbreviations

CFD	Computational fluid dynamics
HiREF	High speed reacting flow research
UTM	Universiti teknologi Malaysia
DT	Detonation tube
DAQ	Data acquisition
DDT	Deflagration to detonation
PT1	Pressure transducer 1
PT2	Pressure transducer 2
AUSM	Advection upstream splitting method
EDM	Eddy dissipation model
A_r	Pre-exponential factor
E_a	Activation energy
H	Hydrogen element
OH	Hydroxyl radical
CEA	Chemical equilibrium with applications
O_2	Oxygen
N_2	Nitrogen
CH_4	Methane
CO_2	Carbon dioxide
RANS	Reynolds-averaged Navier–Stokes
SST	Shear stress transport
NS	Navier–Stokes
k	Turbulence kinetic energy
ω	Specific rate of dissipation
EDC	Eddy dissipation concept
n	Temperature exponent
R	Universal gas constant
O	Oxygen element
RDE	Rotating detonation engine
CJ	Chapman-Jouguet

✉ Mazlan Abdul Wahid
mazlan@utm.my

[1] School of Mechanical Engineering, Faculty of Engineering, High Speed Reacting Flow Research (HiREF), Universiti Teknologi Malaysia (UTM), 81310 Johor Bahru, Johor, Malaysia

[2] Generation Unit, Generation and Environment, TNB Research, 81310 Kajang, Selangor, Malaysia

Introduction

Detonation and deflagration, often known as supersonic and subsonic combustion processes, are the two most prevalent forms of combustion [1, 2]. The detonation mode is triggered by the commencement of a shock wave, which travels

at supersonic speeds through the flammable mixture [3, 4]. The detonation properties, such as high thermal efficiency, quick energy release, and a shockwave across the combustion region, make it a good candidate for power and propulsion research [3]. The field of detonation engines has gotten a lot of attention in recent years because of the potential to surpass the thermal efficiency produced by deflagration-based engines like gas turbines [4–7]. However, the detonation event is a complex interplay of fluid dynamics and chemical kinetics [3]. As a result, there are several major concerns about maintaining detonation propagation in detonation engines, which necessitates appropriate knowledge to aid in the design process of a novel and workable detonation engine.

The detonation properties can be approximated by basic flow models employing the detailed reaction mechanism [8]. The ignition delay time, detonation propagation speed, and other relevant characteristics can all be included in the predictions. However, due to the oversimplification of the flow mechanism, these parameters will require a significant modification for subsequent actual implementations. In most cases, the practical correction is empirical [8]. Using the Computational Fluid Dynamics (CFD) approach, precise mechanisms in the actual reacting and non-reacting flow may be obtained to determine detonation properties [9–12]. Despite breakthroughs in scientific computation that currently allow for direct numerical calculations of complex and multifaceted cellular detonation structures using a detailed chemistry mechanism, this method necessitates a significant amount of computational resources and imposes exceptionally high demands on numerical algorithms in terms of robustness and efficiency. As a result, the use of CFD in combination with detailed chemistry in engineering practice is still limited. For various applications, the amount of detail information that could be extracted from a detailed chemistry computation is not required, therefore a simpler chemical description with a reduced computational cost is recommended [13]. Combining a simplified one-step chemical reaction that can sufficiently capture most of those fundamental physical aspects of multidimensional detonations with a sophisticated CFD solver is very desirable for the engineering design of detonation engines due to the low computer resources required [8, 14].

The established one-step reaction mechanism was developed based on the adjustment of pre-exponential factor and activation energy, and is thus limited to specific reaction circumstances and fuel types [8]. As a result, employing existing mechanisms in a wide range of reaction states can put the computation accuracy into doubt. Westbrook [8] provided a one-step mechanism, which was used to generate an accurate prediction of laminar flame speed under constant atmospheric pressure. The one-step model generates a reasonable prediction when contrasted to the detailed mechanism at different equivalence ratios and fixed initial temperature and pressure. However, this mechanism was created by adjusting the pre-exponential factor and activation energy in the Arrhenius equation while taking into account the laminar flame propagation speed at constant pressure. In the detonation scenario, heat addition occurs in a "constant volume," with heat released from the reaction occurring only in a scant zone after the shock wave. As a result, using a pressure-based one-step model for the detonation scenario would exacerbate the computation discrepancy.

As a result, various publications have begun to develop a one-step mechanism based on the notion of achieving consistent detonation characteristics. One of the underlying principles of developing a reaction model is ensuring that the major detonation parameters are reasonably compatible with the results of the detailed reaction mechanism. Several published works in detonation modelling have already demonstrated the use of a one-step chemistry model rather than detailed chemistry. Yao [15] demonstrated that the one-step model can capture the fundamental macro aspects of a detonation wave, such as the detonation front. The rationale is that they are attempting to determine the basic detonation behaviours and investigate its viability to first order. In a different detonation study, Jin [16] compares the ignition delay time and laminar flame speed of the one-step model for hydrogen and the GRI Mech 3.0 mechanism, as well as experimental data. The ignition delay time in the one-step model is found to be reasonably comparable to that in the GRI Mech 3.0 mechanism. Furthermore, the laminar flame speeds in the one-step model are found to correlate well with the GRI Mech 3.0 mechanism and experimental data. The largest deviations of the one-step mechanism from the experimental data and the GRI Mech 3.0 mechanism are both around 9%.

However, the majority of studies focused on hydrogen-fuelled detonation engines and, as a result, used a hydrogen-oxidizer chemistry model [15, 17–26]. Many studies involving combustion engines have begun to widen the fuel flexibility capabilities by testing different renewable-based fuels [27] such as biogas, as the concept of a non-fossil fuel economy has now become the objective of many regions across the world [28]. Because of its renewable source, biogas has the potential to be one of the alternative fuels for combustion engines. Having said that, there is the possibility of using biogas to power a detonation engine, which should be investigated further. As a result, linking a CFD solver to a simplified one-step global chemical reaction of biogas detonation is highly desirable for the construction of a workable biogas-fuelled detonation engine. Furthermore, the majority of the existing one-step models are based on the interaction of fuel with pure oxygen, which does not match the experimental setup that mainly uses air as an oxidizer with a considerable proportion of nitrogen. To produce a

more precise prediction of detonation properties, the diluting impact of nitrogen must be taken into account.

Hence, the feasibility of one-step irreversible Arrhenius kinetics for the description of biogas detonation is investigated in this work to elucidate the potentiality of this model for use in the development of biogas detonation engines. The current development is based on biogas detonation velocity predictions at varying nitrogen dilutions, which led to a set of optimum chemical-kinetic parameters (temperature exponent, activation energy, and pre-exponential factor) that best fit the biogas detonation velocity obtained in the biogas detonation experiment and the detailed chemistry simulation. That being said, both numerical and experimental setups are used in this study.

Experimental setup

The generation and detection of biogas detonations were executed at the High Speed Reacting Flow Research (HiREF) laboratory, Faculty of Engineering, Universiti Teknologi Malaysia (UTM). The existing detonation tube (DT) facility in HiREF provides a comprehensive set of components for generating and detecting detonation. The facility is made up of the fuel supply system, the air/oxidizer supply system, the DT, the ignition system, and the data acquisition (DAQ) system. Figure 1 displays the schematic for HiREF's DT experimental rig facility.

The facility has been constructed with safety in mind. Due to the tremendous pressure and shock wave produced by the DT, detonation waves can be dangerous to researchers in the facility. The existing DT is housed in a soundproof room and is managed from an outside control room. The DT main body is made up of three tube sections, each section is 0.5 m long and has an internal diameter of 100 mm. One end of the tube is closed while the other is open. The open end through which the detonation wave exhausts into the atmosphere is inserted inside a dampening chamber to minimise the sound produced by the transmitted wave. An extractor device is also installed in the damper chamber to suck up the exhaust gas and unburned mixtures. Two pressure transducers, denoted as PT1 and PT2, were mounted to the DT main body and were placed 560 mm and 750 mm from the ignition source, respectively. The pressure transducer used in the experiment is known as the Kistler 211B300 Piezotron, which produces a high-level, low-impedance signal in terms of voltage analogue of the dynamic pressure input. The major sensing element in the transducer model is crystalline quartz, which is coupled with a solid-state impedance converter. The sensitivity of the transducer ranges from 1.156 to 1.168 mV psi^{-1}. The pressure transducer was positioned atop the cooling adapter to prevent overheating, which might lead to transducer failure. To start a deflagration to detonation (DDT), a series of obstacles were placed in the DT. Figure 2 illustrates the side view of the DT rig setup.

The ignition system was designed to initiate a deflagration before transitioning to a detonation after passing through

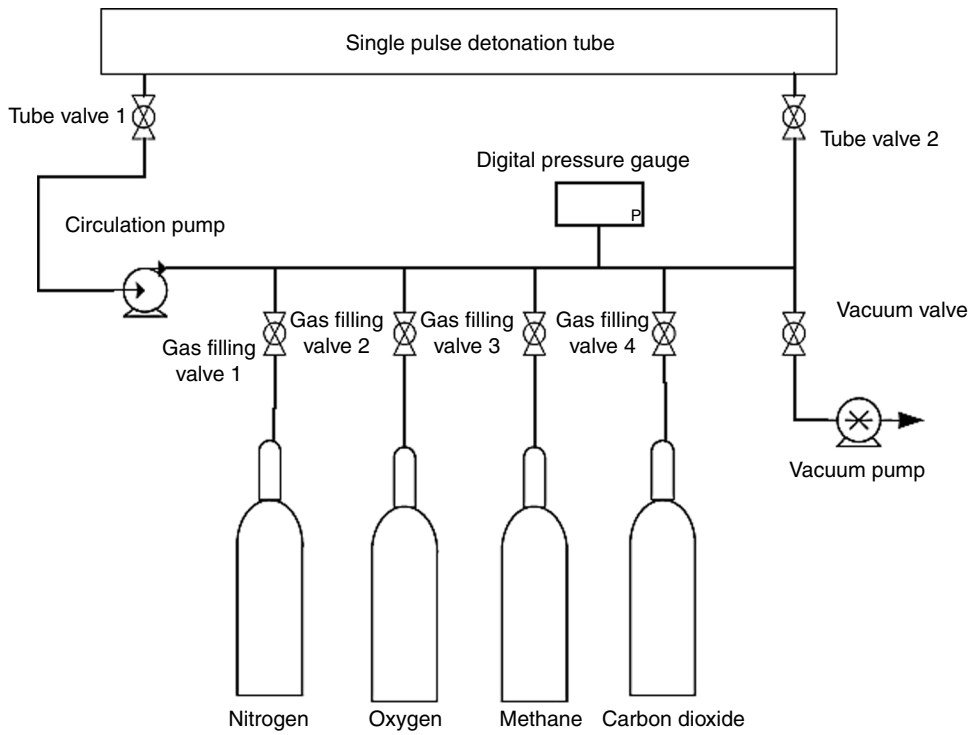

Fig. 1 DT rig facility schematic at HiREF, UTM

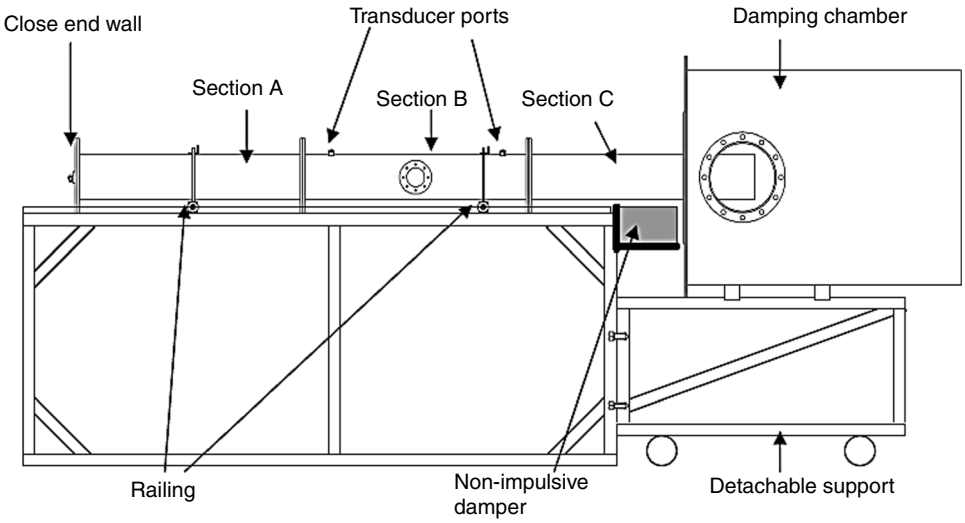

Fig. 2 DT rig facility at HiREF, UTM

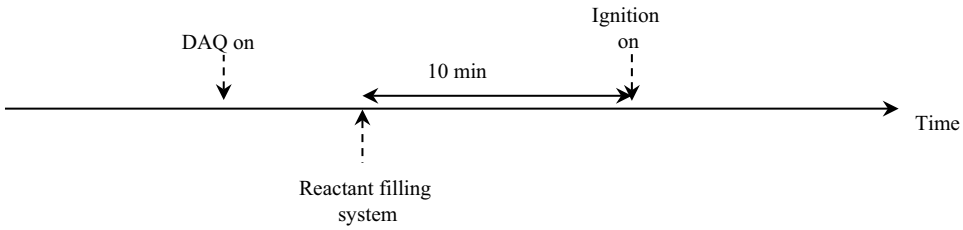

Fig. 3 DT experiment time diagram

the obstacles. The ignition system employs the concept of a discharging capacitor, in which the value of the ignition energy is principally determined by the capacitance value. The ignition value employed in this research is 25 mJ.

The partial pressure approach was used to fill and circulate the biogas-oxidizer mixture in the DT prior to the ignition. The pressure differential caused the reactant to travel from the reactant tanks to the DT since the DT was vacuumed prior to the filling operation. The gauge pressure inlet of the reactant filling is 1 kPa. The experiment was carried out in an ambient environment with a temperature of 302 K. As shown in Fig. 1, the DT main body was connected to a filling system that included a digital pressure gauge, gaseous filling valves, a vacuum pump, and circulation pump valves.

The operating procedures of the reactants filling and circulation system were mostly dependent on the time sequence from the control system. The control system provides an appropriate regulating system to control the timing for the DAQ, filling, and ignition. The Arduino microcontroller executes the controlling functions. Once the signal from the control panel in the personal computer is received by the microcontroller, all of the systems in the DT facility will be activated. The timing sequence is depicted in Fig. 3.

The detonation pressure is the primary parameter of detonation waves collected at the DT facility to continue with the detonation velocity assessment. The detonation velocity from the experimental setup was measured by dividing the distance between PT1 and PT2 with the time required for the combustion wave to propagate between PT1 and PT2. The first arrival of peak pressure following ignition at those pressure transducers was characterized as the arrival of the detonation wave. The data from the transducer was recorded using the DAQ system. All the hardware related to the DAQ system come from the National Instruments. The LabVIEW software is used to display the data recorded by the DAQ system. The digital inputs were acquired directly, whereas the analogue inputs were conditioned and transformed to digital signals for processing by the LabVIEW controller software.

Table 1 Reactant compositions

Composition	C1	C2	C3	C4	C5
CH_4 (%)	65	65	65	65	65
CO_2 (%)	35	35	35	35	35
O_2 (%)	85	75	65	50	35
N_2 (%)	15	25	35	50	65

The experiment was carried out with varied oxidizer (oxygen O_2 and nitrogen N_2) compositions at a constant biogas composition (65% methane CH_4 and 35% carbon dioxide CO_2), as stated in Table 1.

Numerical setup

According to the DT experiment time diagram in Fig. 3, the DT went through a reactant filling and circulation stage for 10 min to guarantee the reactants were adequately mixed. The detonation in the DT is a one-time event. As a result, the numerical analysis was done for a one-time detonation following ignition. In the numerical simulation, the non-reacting flow of the entering reactants was maintained for 10 min based on the filling time, and then ignition began, as shown in Fig. 4.

ANSYS Fluent V19 is used for all setups and numerical processing. To fully reflect the detonation transient phenomena, which is a time-dependent event, the numerical model employed the unsteady, compressible, and reacting Reynolds-averaged Navier–Stokes (RANS) equations without body force. The density-based solver is utilized to simultaneously resolve the governing equations. The density-based solver is a well-known method for modelling supersonic flow [29]. The Shear Stress Transport (SST) k–ω model is employed to resolve the turbulence behaviour. The use of SST k–ω has been shown to produce results that are consistent with the detonation experimental data [30]. In the SST k–ω model, the RANS equations are obtained by splitting the instantaneous flow variables into fluctuating and steady components and applying Reynolds averaging techniques to the Navier–Stokes (NS) equations. Following the Reynolds averaging technique, new terms called Reynold stresses appear, which represent the turbulence effects. Reynolds stresses are resolved via the Boussinesq hypothesis to link the Reynolds stresses to the mean velocity gradients in order to close the RANS equations. The term turbulence viscosity emerges from this relation. To resolve turbulent viscosity, the SST k–ω model is used. Hence, in the SST k–ω model, turbulent viscosity is calculated as a function of the turbulence kinetic energy k and the specific rate of dissipation ω. Detail information on the formulations used in the RANS equations and SST k–ω model can be found in Debnath [1] and Menter [31, 32], respectively.

The convective fluxes are computed using the Advection Upstream Splitting Method (AUSM), a flux-vector splitting approach that is good at providing accurate resolution of contact and shock discontinuities [33]. For the time progression, the four-order Runge–Kutta method is used. Thermal and mass diffusion are both taken into account in governing equations and diffusion coefficients are calculated using the kinetic theory [29]. To resolve the reaction source term in the species continuity equation, the finite rate formulation with the Eddy Dissipation Model (EDM) was used because it has been shown to operate well with the one step mechanism [34]. Ganju [34] contains detailed information on the rate constants and formulas utilised in the EDM. The Eddy Dissipation Concept (EDC) was chosen for the detailed

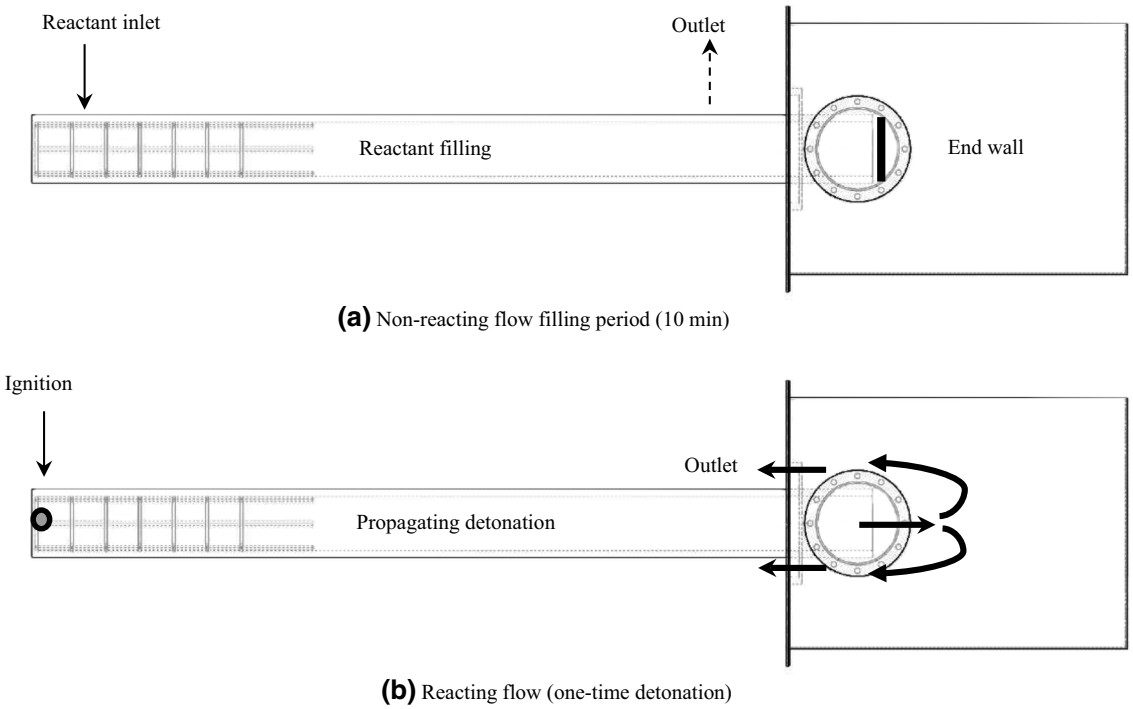

Fig. 4 Overall DT numerical process. **a** Non-reacting flow filling period (10 min) **b** Reacting flow (one-time detonation)

chemistry simulation because it works well with the detailed chemistry mechanism [34].

Model chemistry

The effect of chemical kinetics is then modelled in the species continuity equation by executing a comprehensive validation feedback loop process to acquire the optimum set of chemical-kinetic parameters (activation energy, pre-exponential factor, and temperature exponent) which fit best the biogas detonation velocity acquired from the biogas detonation experiment and the detailed chemistry simulation. The rate of chemical energy release is mostly influenced by the chemical kinetics model. The generation of chemical energy, which is also represented in the change in the internal energy of the biogas-air mixture, has an effect on the flow gas dynamics, determining the detonation wave velocity [3]. The chemical kinetics are expressed by a one-step irreversible Arrhenius rate law *Reactant* → *Product,* as shown in Eq. 1. The reaction progress is described by an Arrhenius rate law [3], as given in Eq. 2 [30, 33, 35],

$$CH_4 + 2O_2 \rightarrow CO_2 + 2H_2O \tag{1}$$

$$k_r = A_r T^n e^{-E_a/RT} \tag{2}$$

where A_r is the pre-exponential factor which defines the spatial and temporal scales, n is the temperature exponent, E_a is the activation energy, and R is the universal gas constant. Due to its simplicity, such a model has been largely considered in many detonation simulations, while retaining certain crucial elements such as the temperature sensitivity provided by the global activation energy.

In a one-step model involving detonation states, the E_a is the main parameter controlling the sensitivity of the reaction zone and the bifurcation parameter describing the stability of the detonation front. However, as several studies [3] have pointed out, this may not be a sufficient parameter. Therefore, three primary kinetic parameters, n, A_r, and E_a, were explored in the current study in order to provide a comprehensive set of chemical-kinetic parameters for biogas detonation velocity.

As the contemporaneous existence of CH_4 and CO_2 can alter the chemical behaviour of the entire system in an unanticipated manner, the one-step model that stays reasonably accurate in the presence of dilution is of primary importance. When comparing Eq. 1 to the biogas-air mixture used, additional reactant species, such as CO_2 and N_2, act as non-participating species. CO_2 and N_2 have a major part in the diluting action of the reactant, which lowers the energy density [36]. Hence, it will not participate in the chemical process. And the absence of these species from the chemical reaction is acceptable since the detonation pressure and velocity, not the species of detonation products, are the key determinants of the optimum kinetics parameters. As a result, while CO_2 and N_2 have a non-participating influence in the chemical process, their inclusion as a diluting factor remains in the domain. The tuning of kinetic parameters in Eq. 1 and Eq. 2 for biogas detonation will ensure that the chemical behaviour change caused by the simultaneous presence of CH_4 and CO_2 can be adequately captured to imitate the actual biogas detonation velocity from the experiment.

Grid-convergence analysis

Prior to the execution of a validation feedback loop process to acquire the optimum set of chemical-kinetic parameters, three convergence accuracy assessments were performed in the current study to reduce numerical systematic errors, including spatial, temporal and iterative convergence accuracies. The reactant composition used for the convergence accuracy tests is C1, as shown in Table 1, with the baseline kinetic parameters are 2×10^{15} s^{-1}, 0, 14,644 J mol^{-1}, and 8.314 J (mol.K) $^{-1}$ for A_r, n, E_a, and R, respectively [37].

Spatial convergence accuracy: mesh quality and mesh independent test

The DT computational domain has been discretized using the Assembly Meshing method, with hexahedral-dominant meshes. To confirm that the prediction results are unaffected by the amount of meshes created, a mesh independent test is carried out. Table 2 summarizes the characteristics of the various meshes that have been used in the DT computational domain. As the level of spatial discretization error is also affected by the mesh quality, meshes are generated with orthogonal quality and skewness taken into account to represent the mesh quality [38]. The orthogonal quality represents how close the angles between adjacent mesh faces are to the optimal angle. The range for orthogonal quality is 0 to 1, with a value of 1

Table 2 Characteristics of the various meshes being used

Average element size/mm	Grid points	Meshes (10^6)	Orthogonal quality	Skewness
0.7	1.075	1.031	0.937	0.088
0.5	1.602	1.570	0.942	0.091
0.3	2.691	2.470	0.935	0.087
0.2	2.703	2.650	0.944	0.095
0.05	3.075	3.010	0.945	0.092

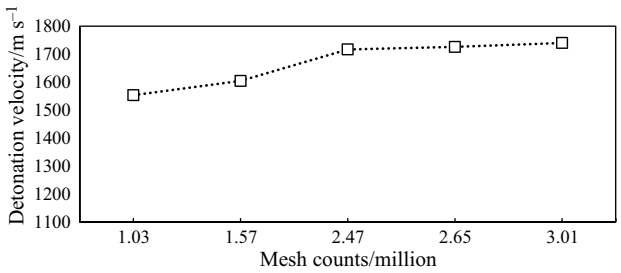

Fig. 5 Detonation velocities in the DT at varying mesh counts

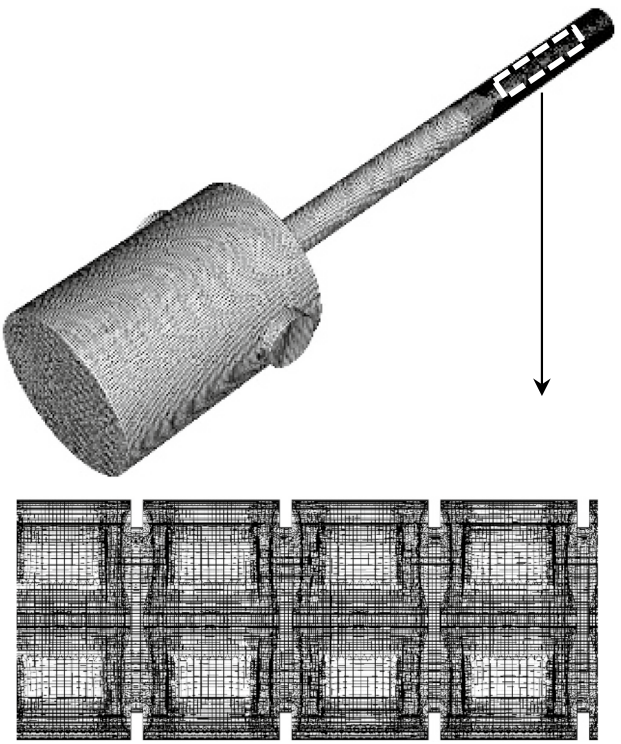

Fig. 6 DT mesh model

being the best quality [38]. The skewness on the other hand, represents how close the mesh to the ideal equiangular mesh is. Highly skewed faces and meshes are unacceptable as the governing equations being solved assuming that the meshes are relatively equiangular. The range for skewness is 0 to 1, with a value of approaching zero has the lowest deviation from a normalized equiangular angle [38]. As seen in Table 2, all the generated meshes was controlled to get the high quality of average orthogonal and average skewness.

Figure 5 shows the detonation velocity values in the DT as the mesh count changes. The detonation velocity nearly no longer varies when the mesh number increases from 2.65 to 3.01 million, with a variation of less than 1%. Hence, 2.65 million meshes are chosen for the DT model.

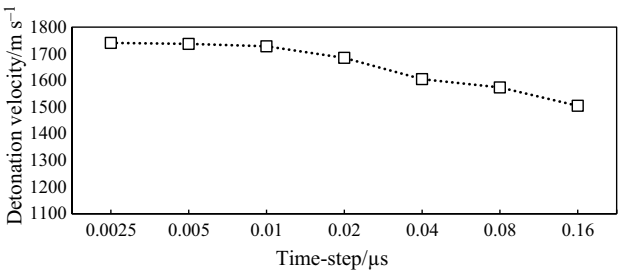

Fig. 7 Detonation velocities in the DT at varying time steps

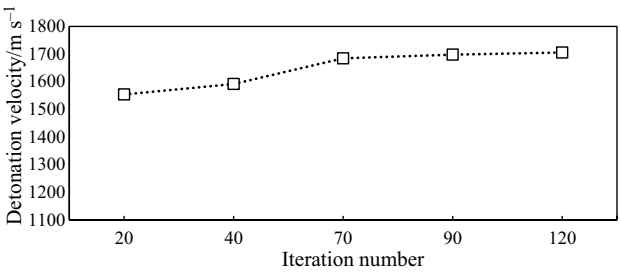

Fig. 8 Detonation velocities in the DT at varying iteration numbers

Figure 6 depicts the independent mesh model of the DT domain. Since the detonation transition from deflagration involves intricate interrelationships of flame front, shock front, turbulence dynamics, and boundary layers [39–41], the upstream domain region, where the obstacles are located to generate DDT, has a more refined mesh than the downstream domain area.

Temporal convergence accuracy: time-step independent test

Time-accurate simulations require discrete time-steps that must be examined to ascertain the sensitivity of the simulation results to the size of the time-step. Hence, the temporal discretization error for DT modelling was examined at various time-steps, as shown in Fig. 7. With a variation of less than 1%, a time-step of 0.01 μs is chosen for the DT modelling.

Iterative convergence accuracy: iteration number independent test

The accuracy of iterative convergence accuracy was performed by the determination of the independent number of iterations needed to advance to a new time-step. Therefore, the iterative convergence errors for DT modelling was assessed at various iteration numbers, as shown in Fig. 8,

respectively. With a variation of less than 1%, an iteration number of 90 is chosen for the DT modelling.

Results and discussion

Figure 9 depicts the findings of biogas detonation velocities from experiments and detailed chemistry (GRI Mech 3.0) simulations. The experimental results, detailed chemistry simulations, and the impact of kinetic parameters for the one-step model were all examined in depth in subsequent sections.

Experimental results

The synergistic effect of N_2 and CO_2 dilution on detonation is to lower the total energy release of the biogas-air mixture, resulting in a decrease in detonation velocities and thus shock temperatures, as shown from the experimental results in Fig. 9, where there is a significant drop in the biogas detonation velocity as the N_2 percentage increases to 50%. However, the addition of CO_2 raises the specific heat capacity of the mixture, which has the reverse effect of raising the shock temperature. The experimental results show that these two contrasting effects are roughly balanced, therefore the detonation velocity does not change considerably with 15–35% N_2 dilution.

According to the findings of the experiments, the range of biogas detonation velocity with 15–35% and 50–65% N_2 dilutions is 2000 to 2100 m s^{-1} and 900 to 1000 m s^{-1}, respectively. As a result, as the dilution of N_2 in the oxidizer increases to 50%, the biogas detonation velocity decreases by approximately 50%. The considerable decrease in biogas detonation velocity with 50% N_2 dilution could potentially be attributed to the suppression of hydrodynamic instability. It is widely assumed that the initiation of detonation is caused mostly by hydrodynamic instability. The increase in flame surface density is the cause of hydrodynamic instability, and various studies have shown that the intensity of hydrodynamic instability is directly connected to the thermal expansion ratio, which is defined as the ratio of unburned gas density to burned gas density [42]. It is widely acknowledged that the bigger the thermal expansion ratio, the greater the hydrodynamic instability. Previous research has demonstrated that the thermal expansion ratio decreases uniformly as CO_2 dilution increases [42]. Furthermore, in the current experiment, the CO_2 and N_2 operate jointly, causing the thermal expansion ratio to drop far more than when CO_2 operates alone. Given that a higher thermal expansion ratio enhances hydrodynamic instability, increasing N_2 dilution substantially inhibits hydrodynamic instability, resulting in a lower detonation velocity.

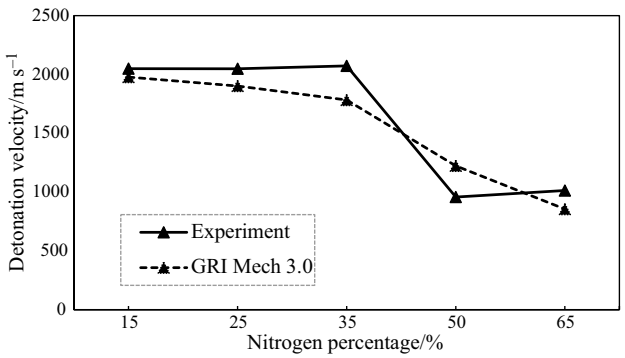

Fig. 9 Biogas detonation velocities from experimental and GRI Mech 3.0 simulation results

Another possible explanation for the considerable decline in detonation velocities during the 50–65% N_2 dilutions is the decoupling of the reaction zone and the leading shock front of the detonation wave. This is corroborated by prior findings from the literature, which show that at more than 50% dilution, the reaction zone decouples completely from the leading shock front [3]. This decoupling occurs when there is insufficient heat of reaction behind the shock front, allowing the reaction rate to not closely follow the shock front. The heat emitted behind the shock front functions as an energizer, propelling the shock front forward. A greater heat energy release pulse improves energy release coherence and is less vulnerable to flow disturbance, resulting in stronger detonation wave propagation. The energy released behind the shock front is greater when the detonation consumes the biogas-oxidizer mixture with 15–35% N_2 dilutions than when the detonation consumes the biogas-oxidizer mixture with 50–65% N_2 dilutions.

Heat loss to the DT walls is also one of the causes of a severe velocity deficit, however its influence may not be as strong as the dilution impact. It is well understood that flame acceleration is a vital element in the DDT. The amount of heat loss at walls increases when the flame first accelerates to detonation due to the high-temperature zone at the DT walls, which is lengthy in size. The detonation then begins to decelerate and generates an expansion wave ahead of it. With increasing dilution, the heat release behind the detonation front decreases, resulting in the heat release being unable to balance the heat loss to the DT walls, causing the detonation velocity to suffer substantial degradation as it reaches 50% N_2 dilution.

Detailed chemistry results

The GRI mechanism was chosen for a detailed chemistry simulation of biogas detonation because it has already been found to perform well when compared with biogas

experiment results and has been well validated elsewhere [43]. Figure 9 depicts the trend in biogas detonation velocity in a detailed chemistry simulation using the GRI mechanism (GRI Mech 3.0), which exhibits a gradual decrease as N_2 dilution increases. The decrease in detonation velocities is more uniform as compared to experiment results. The biogas detonation velocity is predicted to be lower in the region of 15–35% N_2 dilution as compared to the experiment, with a percentage decrement of 3–14%. In contrast, with 50–65% N_2 dilution, there are slight predictions in the biogas detonation velocity as compared to the experiment, with a percentage increment ranging from 15 to 28%. The percentage differences with the experiment from 15 to 35% N_2 dilution are lower than from 50 to 65% N_2 dilution. One of the reasons for this is that the O_2 percentage is higher in the 15–35% N_2 dilution, resulting in a leaner and near stoichiometric condition. It is widely known that the GRI mechanism was specifically designed to capture the combustion of hydrocarbon (mainly CH_4) and has been proved to satisfactorily characterise lean and stoichiometric combustion [43]. As a result, there is a good chance that lowering the O_2 percentage in 50–65% N_2 dilution will result in a richer condition, lowering not only the detonation velocity due to insufficient O_2 to complete the biogas reaction, but also the prediction accuracy of the GRI mechanism to tailor for a richer fuel state. Nonetheless, four of the five N_2 percentage cases illustrated in Fig. 9 had a disparity of less than 15% when compared to the experimental data. Furthermore, the drop in biogas detonation velocity follows the same qualitative trend reported in the experiment data. As a result, the GRI mechanism can be deemed suitable for biogas detonation modelling and can assist in the development of one-step chemistry.

The chain-branching kinetics and exothermic recombination are well interpreted in the set of detailed chemistry reactions. The reaction zone length behind the shock front is closely related to the chain-branching and recombination kinetics of the oxidation scheme. The length of the reaction zone increases as the amount of dilution increases due to alterations in the elementary rates at the end of the chain-branching phases and during the recombination stages of the oxidation process [3]. In biogas, the presence of CO_2 in the fuel and N_2 in the oxidizer acts as a diluting factor, resulting in a significant reduction in total heat release and a lower temperature gain in the reaction zone. Because of the lower temperature in the reaction zone, the chemical reaction rates of exothermic reactions slow down, resulting in an increase in heat release times. That being said, the lengthening of the reaction zone during detonation is caused by an increase in heat release timings. As a result, dilution has the primary effect of lengthening the reaction zone behind the shock front. The peak temperature of the reaction zone decreases as dilution increases and heat release times increase [3]. Subsequently, the creation of radicals from the chain-branching reaction will be too sluggish to sustain the necessary coupling with the exothermic section of the reaction structure to drive the detonation wave. As a result, the reaction zone separates from the shock and the detonation ceases. Overall, increasing N_2 dilution reduces detonation velocity significantly due to a significant decrease in the chain-branching reaction rate, which lowers the production rate of important free radicals such as H, O, and OH. These radicals are known to have an important part in the detonation creation [42].

With 50% N_2 dilution, there is a difference in detonation velocities between the experiment and the prediction from detailed chemistry simulation with approximately 28% discrepancy. One of the possible factors is the computation of the turbulence-chemistry model in the simulation. Although the turbulence-combustion model used in the current study provides the optimal balance between the accuracy and efficiency of the numerical simulation, the hydrodynamic instability, which is one of the major mechanisms for the occurrence of detonation, cannot be captured with great precision through the present model. Hydrodynamic instability is the result of complicated interactions between flow and surrounding boundaries, as well as the resulting flame unburned gas flow feedback mechanism, which initiates turbulent flow ahead of the flame front, increasing the flame surface and velocity [44]. That being said, a genuine detonation wave front is highly corrugated as a result of turbulence and a very non-uniform fuel–air mixture processed by the wave. The current study's turbulence dynamics was modelled using the RANS method, which generates average solution that ignores out any fluctuation of scalar and vector fields [46], reducing the vorticity production mechanisms [45], which is one of the main components to prompt the hydrodynamic instability [44]. This could result in significant local differences in detonation wave velocity, as well as post-detonation pressures and temperatures. Hence, at 50% N_2 dilution, the precise influence of dilution may not be adequately predicted in the simulation due to the restriction of the present turbulence-chemistry model to adapt for a higher dilution because the concurrent presence of CO_2 from biogas and a high N_2 percentage in the oxidizer could affect the chemical interactions of the entire system in an unexpected fashion. Nonetheless, because the current study does not focus on the detonation structure, the RANS formulation is sufficient to provide essential macro insights on the detonation velocity.

The disparity in detonation velocity at 50% N_2 dilution could also potentially be attributable to the assumption used in the current simulation, which ignored heat loss to DT walls by assuming no heat transfer at the DT surfaces. This is not an unrealistic assumption, given the high heat capacity and thermal conductivities of steel-clad DT walls. As a result, when compared to the temperature of the hot detonation wave products, the temperature rise in one detonation

cycle can be deemed relatively moderate. Nonetheless, this assumption is mainly appropriate for single-pulse DTs [46], which is what is used in this study. The wall temperatures will be higher for multiple-cycle detonation operations of long duration, as would be encountered in rotating detonation engine (RDE) applications, due to the increase in heat loss rate, and thus for RDE cases, the exact level of heat loss to the wall will be dependent on wall cooling methods. Nonetheless, according to a prior study, heat loss through the wall accounts for only about 10% of the entire detonation velocity deficit [47]. Only in micro-scale channels (about 0.1 mm) does heat transmission to walls have a substantial effect on flame acceleration and DDT [48]. The heat-loss impact is weaker in a wider channel, such as the DT used in this study, where viscosity and inertial influences are more dominant. Hence, we estimate that heat losses to walls are minimal and thus omitted in the current heat-loss model. All in all, the current modelling explicitly accounts for just the exothermicity within the reaction zone structure and ignores the endothermicity induced by heat losses to the wall.

One-dimensional Chapman-Jouguet (CJ) detonation results

Before assessing the kinetic parameters for the one-step model based on experimental and detailed chemistry simulation results, a comparison of these findings with CJ detonation velocities obtained from one-dimensional simulations via NASA CEA code was performed to assess overall results consistency, as shown in Fig. 10. Gordon [49] goes into great detail about the approach of establishing equilibrium compositions for the calculation of CJ detonations in the NASA CEA algorithm. Given the three-dimensional effect, it stands to reason that the majority of the N_2 dilution cases predicted by detailed chemistry simulations have lower detonation velocities than that predicted by the CEA algorithm. The percentage discrepancies with detailed chemistry simulation results vary from 0.3 to 14.9%, indicating near concordance with detailed chemistry results. However, when compared to the experimental results, there is a considerable range of percentage discrepancies ranging from 3 to 48%. Discrepancies with experimental data are greater at 50–65% N_2 dilution.

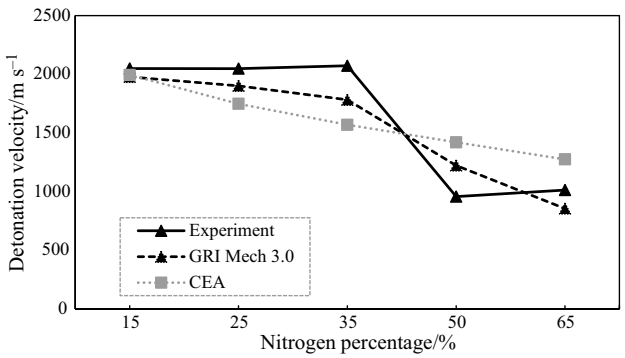

Fig. 10 Biogas detonation velocities from experimental, GRI Mech 3.0 simulation, and CEA results

One of the main reasons for these considerable percentage differences is that the one-dimensional computation does not account for external factors such as heat loss to the ambient and nearby walls, as previously discussed. Furthermore, the CJ detonation parameter calculation assumes that the transformation of the explosive reactants into products occurs over an infinitesimal thin surface and that the chemical events occur instantaneously [3]. With these assumptions, the products behind the detonation front are thermodynamically equilibrium, and their properties can be calculated using the standard thermodynamics formula [3]. Hence, the theory's simplicity hinders one from obtaining an interrelationship of the reaction zone and shock front zone of the detonation fronts, where the CJ detonation calculations assume the shock front instantly affects the conversion of the chemical composition in the reactive mixture without the inclusion of the reaction zone behind it. As a result, the impact of dilution, which mostly affects the reaction zone, will not be well reflected by the one-dimensional CJ detonation calculation. Furthermore, the simplicity of the theory prevents the turbulence-chemistry influence from being included in the CJ detonation calculation, which further increases the discrepancy. Nonetheless, for all results, the decline in detonation velocity may be deemed consistent with an increase in N_2 dilution, demonstrating the reliability of the results obtained from the experimental and detailed chemistry simulation data.

One-step chemistry: temperature exponent impact

To prevent numerical stiffness in the computation [13], a narrow range of n values between 0.0 and 0.2 was used at fixed baseline values of A_r, E_a, and R. Figure 11 shows the prediction of biogas detonation velocities at varying n values. When n in Eq. 1 was set to zero, the reaction substantially underestimated the detonation velocity when compared to experimental results and numerical predictions based on the detailed chemistry mechanism of GRI Mech 3.0. One of the primary reasons for the extreme underestimation of biogas detonation velocity at $n = 0$ is because the baseline one-step model was originally designed for the reaction between pure CH_4 and pure O_2. However, because the current study focused on detonation from a biogas-air mixture, the addition of CO_2 (from biogas) and N_2 (from oxidizer) increases the dilution effect of the reactant and reduces the

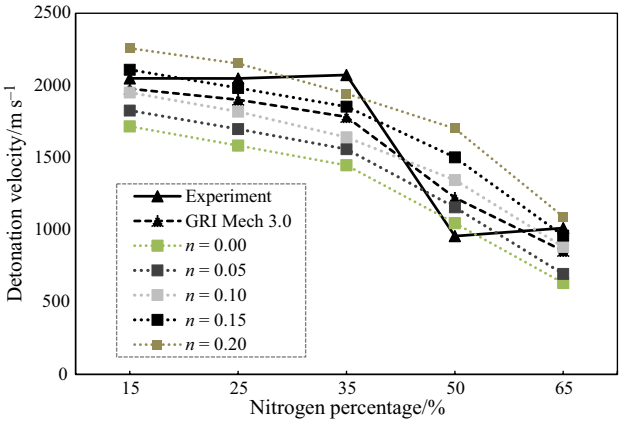

Fig. 11 Prediction of biogas detonation velocities at varying n values

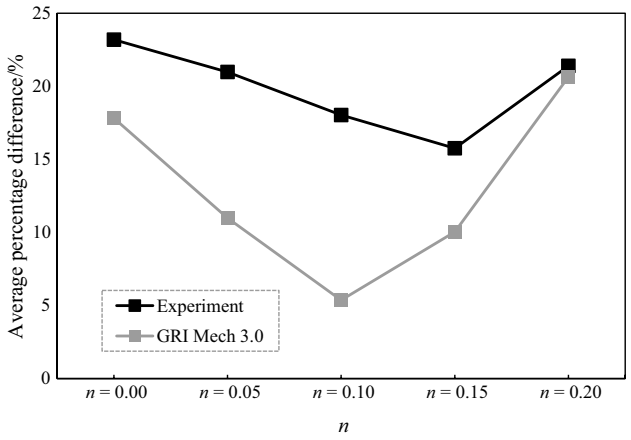

Fig. 12 Percentage differences of detonation velocities with experimental and GRI Mech 3.0 results at varying n values

energy density even further. As a result, the original one-step model ($n=0$), as shown in Fig. 11, does not account for the dilution effects of CO_2 and N_2, resulting in a substantially lower detonation velocity when compared to experiment results and detailed chemistry simulation. Therefore, as the n value grows, so does the reaction rate and the detonation velocity.

The size of the hot area anticipated by the chemistry model also has a significant impact on detonation predictions. The results in Fig. 11 are consistent with Wang [50], who found that the area of a hot spot with a temperature gradient capable of causing a detonation in simulations using a detailed chemistry model can be orders of magnitude bigger than that in simulations using a one-step model. To explain the situation, it is crucial to note that many researchers have stressed that an extensive description of the details of the chemical pathways (detailed chemistry) is unneeded for many practical scenarios [51]. Instead, it is more critical to have a fluid dynamics model coupled to a chemical-energy release model that places the released heat energy in the "right" place in the flow at the "right" moment [51]. However, according to the assumptions for the one-step model, the reaction is practically exothermic at all temperatures. The actual chemical properties of the reaction structures behind detonation fronts, which are often regulated by chain-branching kinetics, cannot be reproduced by a single Arrhenius reaction model. In particular, one-step Arrhenius kinetics cannot modulate the two major characteristic zone lengths, the induction length and the primary heat release length [13].

The induction phase and the exothermic period, during which radicals recombine to create products, make up the chain-branching reaction structure [3]. The induction process in chain branching kinetics event is an endothermic scenario in which energy is absorbed to break the reactant species and generate radical species. As a result, for a detailed chemistry mechanism, the heat released during this induction period is practically "zero". That being said, unlike a detailed chemistry mechanism, a single Arrhenius reaction model does not have a chain-branching-thermal explosion characteristic. Hence, applying detailed chemistry in a simulation actually necessitates a lower temperature differential to activate the reaction than predicted by the original one-step model. This is due to the "absence of heat emitted" during the induction period, which shortens the period of heat energy release and increases the peak magnitude of heat released. As a result, the size of a hot spot/magnitude of heat release caused by a temperature gradient in simulations with a detailed chemistry model can be orders of magnitude bigger than in simulations with the original one-step model ($n=0$). Therefore, another rationale for increasing the n value is to ensure that the size of the induced hot spot rises, potentially boosting the detonation intensity and properly replicating biogas detonation results from the detailed chemistry simulation.

The average percentage difference for each n value with the experimental results and the simulation using GRI Mech 3.0 mechanism was measured and shown in Fig. 12 in order to select the most suitable n value for developing the one-step model that can correspond well with both experimental and GRI Mech 3.0 simulation results. The n value 0.15 produced the lowest average error of all n values tested with 15.76% and 10.03% (both percentages fell below 16%) when compared with the results of experimental and GRI Mech 3.0, respectively.

One-step chemistry: activation energy impact

To complete the formulation of the one-step model, the activation energy E_a is the next parameter to go through the validation feedback loop. When making a selection based on biogas detonation velocities results, one should take note that the E_a influences the sensitivity of the reacting flow response to temperature changes in one-step Arrhenius kinetics. Furthermore, the direct exponential interrelationship between the overall reaction rate and E_a may have an unanticipated detrimental effect on the already complex detonation behaviour. As a result, the progressive increment from the baseline E_a value was deliberately done on purpose to avoid a dramatic rise in the difference between the experimental and detailed chemistry simulation results.

Figure 13 depicts the prediction of biogas detonation velocities at varying E_a values with constant baseline values of A_r and R, as well as the n value of 0.15 established previously by the validation feedback loop. Prior to the validation feedback loop to determine the optimal E_a value, a selection from different multiplier values was made to ensure that the E_a value did not suddenly spike from the baseline value. As there is a reasonable leap in reaction rate and detonation velocity with increasing E_a value, a multiplier of 1.05 was used to provide the increment of E_a starting from the baseline value.

At N_2 dilutions of 15–25%, the detonation velocities jump to more than 2300 m/s for high E_a values (16,952 and 17,800 J mol^{-1}). The thermodynamic condition of the reaction zone behind the detonation fronts is highly reliant on the reaction rate at high E_a values [52], resulting in a significant rise in detonation velocities. Which is also why there is a drastic dip in detonation velocity when N_2 dilution is increased to 50–65% in high E_a cases over low E_a cases. Because the reaction rate is greatly influenced by the thermodynamic state, the reaction zone length grows rapidly as the shock front speed drops due to the dilution effect. Hence, the reaction zone may detach from the shock wave, resulting in lower detonation velocities. That being stated, high E_a values have higher sensitivity with dilution increments. In low E_a cases (14,644, 15,376, and 16,145 J mol^{-1}), the reaction rate is less dependent on the thermodynamic state than that in high E_a cases. As a result, there is a gradual decrease in detonation velocities as N_2 dilution increases, rather than a rapid decrease as seen in high E_a instances.

Overall, it has been discovered that when the E_a grows, the magnitude of the detonation velocity increases. With rising E_a, the high temperature sensitivity of the reactant may induce a violent explosion when the pre-compressed reactant meets the shock front medium, resulting in a higher overdriven detonation intensity than with low E_a.

In order to select the most suitable E_a value for developing the one-step model that can correspond well with both experimental and GRI Mech 3.0 simulation results, the average percentage difference for each E_a value with the experimental results and the simulation using GRI Mech 3.0 mechanism was measured and shown in Fig. 14. While the average percentage difference with GRI Mech 3.0 results grows as the E_a value rises, the average percentage difference with experimental data decreases as the E_a advances from 14,644 J mol^{-1} to 16,145 J mol^{-1}, before intensifying as the E_a rises further. As a result, the selected E_a value is 16145 J mol^{-1}, as both percentage discrepancies are shyly below 15%.

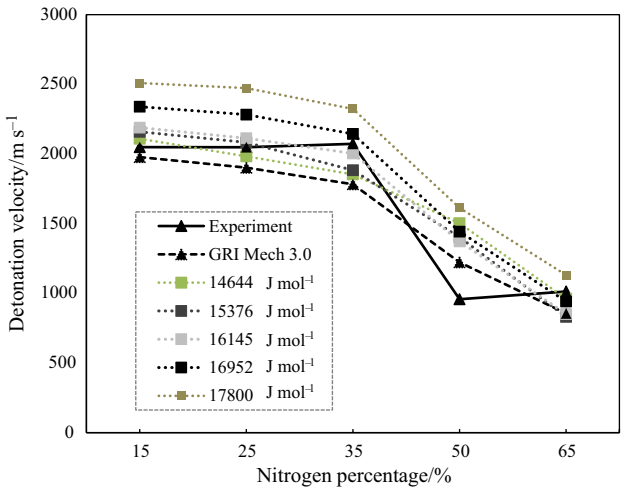

Fig. 13 Prediction of biogas detonation velocities at varying E_a values

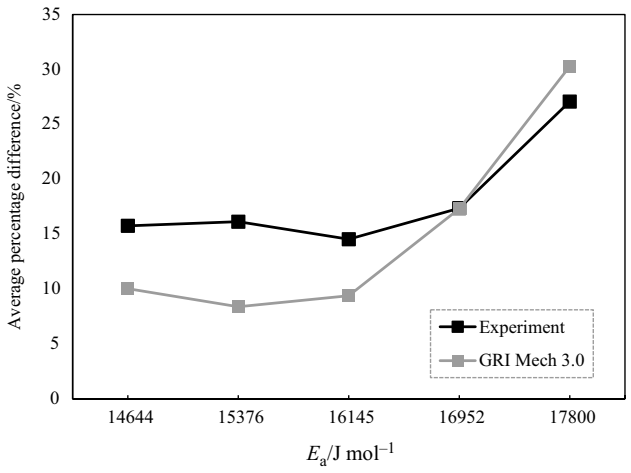

Fig. 14 Percentage differences of detonation velocities with experimental and GRI Mech 3.0 results at varying E_a values

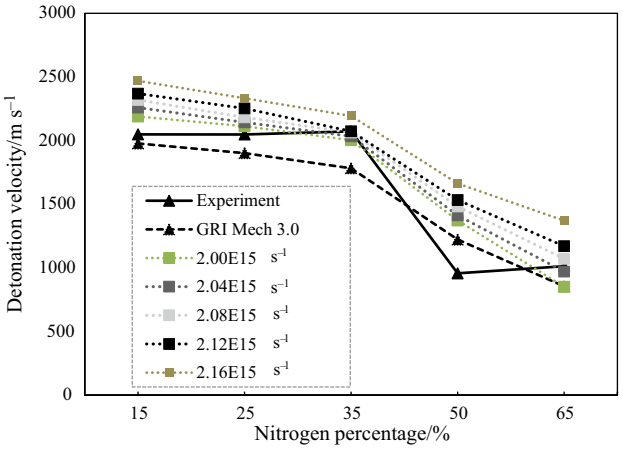

Fig. 15 Prediction of biogas detonation velocities at varying A_r values

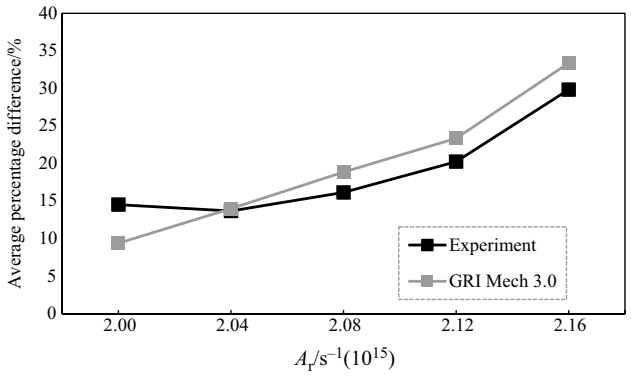

Fig. 16 Percentage differences of detonation velocities with experimental and GRI Mech 3.0 results at varying Ar values

One-step chemistry: pre-exponential factor impact

The pre-exponential factor A_r is the final parameter to complete the one-step model formulation. The validation feedback loop for A_r was implemented in a small range to avoid a major rise in the discrepancy between the experimental and detailed chemistry simulation results, as the explicit temperature dependence of the A_r had already been implemented via the earlier selection of n value. The final validation feedback loop was used to determine the best value for A_r in order to see whether there was any possibility to further reduce the percentage disparity between experimental and detailed chemistry results.

Figure 15 shows the prediction of biogas detonation velocities with varied A_r values, with constant R, as well as the n value of 0.15 and E_a value of 16,145 J mol^{-1} established previously via validation feedback loops. Since the reaction rate and detonation velocity vary as the A_r value increases, a multiplier of 1.02 was chosen to provide a gradual increase in A_r from the baseline value.

According to Fig. 15, in terms of the overall pattern of biogas detonation velocity degradation as N_2 dilution increases, increasing A_r has relatively maintained the decrement pattern of detonation velocity. As A_r is the pre-exponential constant in the Arrhenius equation, there is a direct empirical relationship with the overall rate constant. As a result, there is a relatively uniform gradient of velocity reduction with the increase of A_r as opposed to the increase of E_a, which is temperature sensitive to the reaction rate, allowing the reaction zone behind the shock front to be highly dependent on E_a value, and resulting in a significant decline in biogas detonation velocity as it reaches more than 50% N_2 dilution (Fig. 13). Nonetheless, increasing A_r to 2.04×10^{15} s^{-1} succeeded to further reduce the percentage discrepancy with experimental and detailed chemistry simulation results, with 13.7% and 14.0%, respectively, as shown in Fig. 16.

Conclusions

We have demonstrated how the effects of N_2 dilution can be successfully incorporated into a simple one-step Arrhenius model by considering variable values of n, E_a, and A_r into account, with the proposed model describing biogas detonation velocity with sufficient accuracy (< 15% discrepancy). Out of the three parameters under consideration, an increase in E_a managed to generate a significant dip in biogas detonation velocity as the N_2 dilution reached 50% dilution, which was also captured in the current biogas detonation experiment, demonstrating that the dependence of high and low E_a values could appropriately tailor for changes in the thermodynamic condition of the reaction zone behind the detonation fronts as the N_2 dilution increased.

The detailed chemistry from the GRI mechanism has been demonstrated to reliably predict the biogas detonation velocity, with most N_2 dilution cases having less than 15% discrepancy when compared to experimental data, except for the case of 50% N_2 dilution, which had a 28% discrepancy. Aside from the assumptions employed (neglected heat loss to walls, simplicity in the turbulence-chemistry interaction), the GRI mechanism's prediction accuracy has exhibited a slightly reduced ability to tailor for a richer fuel state (decrease in O_2), as observed in the high N_2 percentage cases. Nonetheless, the decrease in biogas detonation velocity follows the same qualitative pattern as the experiment data. As a result, the GRI mechanism can be considered suitable for biogas detonation modelling, and it was able to aid in the establishment of one-step Arrhenius chemistry for biogas detonation velocity, together with experimental data.

The proposed one-step would undoubtedly contribute significantly to a more realistic condition during the design phase of a detonation-based engine, when a shorter simulation period is preferred. As a result, it has the potential to be combined with a digital twin system for a future biogas-fuelled detonation engine system in order to monitor detonation performance as operating conditions are changed. The way forward is to further increase the reliability of the said model by broadening the parameters of interest, which include detonation temperature and pressure.

Acknowledgements The authors would like to acknowledge their gratitude to High Impact Research (HIR) Grant UTM vote number 09G05 and Transdisciplinary Research (TDR) Grant UTM vote number 01 for the funding of the project.

Author contributions All authors contributed to the study conception and design. Mohammad Nurizat Rahman was in charge of material preparation, data collection, numerical work, and major analysis. Mohd Haffis Ujir was in charge of the experiment. Mohammad Nurizat Rahman wrote the first version of the manuscript, and all contributors provided feedback on prior versions. Mazlan Abdul Wahid is the grant project manager for the current study. Mazlan Abdul Wahid, with the assistance of Mohd Fairus Mohd Yasin, is the principal research supervisor for this study. The final manuscript was read and approved by all authors.

Research funds: High Impact Research (HIR) Grant UTM vote number 09G05 and Transdisciplinary Research (TDR) Grant UTM vote number 01.

References

1. Debnath P, Pandey KM. Numerical analysis of detonation combustion wave in pulse detonation combustor with modified ejector with gaseous and liquid fuel mixture. J Therm Anal Calorim. 2021. https://doi.org/10.1007/s10973-020-09842-1.
2. Rahman MN, Wahid MA, Yasin MFM, Abidin U. Predictive numerical analysis on the mixing characteristics in a rotating detonation engine (RDE). Evergreen. 2021. https://doi.org/10.5109/4372268.
3. Zhang F. Shock waves science and technology library (vol. 6). Berlin; 2014
4. Zhang X, Gui M, Pan Z, Zhang H. Numerical investigation on the rotating detonation critical mode for a methane–air mixture in an annular tube using reactive Navier-Stokes equations. J Therm Anal Calorim. 2021. https://doi.org/10.1007/s10973-020-10406-6.
5. Alam N, Sharma KK, Pandey KM. Numerical investigation of flame propagation in pulse detonation engine with variation of obstacle clearance. J Therm Anal Calorim. 2019. https://doi.org/10.1007/s10973-019-08948-5.
6. Mazlan MA, Yasin MFM, Saat A, Wahid MA, Rahman MN. Initiation characteristics of rotating supersonic combustion engine. Evergreen. 2021. https://doi.org/10.5109/4372275.
7. Rahman MN, Wahid MA, Yasin MFM. Predictive numerical analysis on the fuel homogeneity in a rotating detonation engine (RDE) implementing radially- entered fuel injection scheme. IOP Conf Ser : Mater Sci Eng. 2020. https://doi.org/10.1088/1757-899X/884/1/012109.
8. Wang B, Wei W, Ma S, Wei G. Construction of one-step H_2/O_2 reaction mechanism for predicting ignition and its application in simulation of supersonic combustion. Int J Hydrog Energy. 2016. https://doi.org/10.1016/j.ijhydene.2016.09.010.
9. Dong H, Zan W, Hong T, Zhang X. Numerical simulation of deflagration to detonation transition in granular HMX explosives under thermal ignition. J Therm Anal Calorim. 2017. https://doi.org/10.1007/s10973-016-5772-4.
10. Rahman MN, Yasin MFM, Aris MA. Reacting flow characteristics and multifuel capabilities of a multi-nozzle dry low NO_x combustor: A numerical analysis. CFD Lett. 2021;13(11):21–34. https://doi.org/10.37934/cfdl.13.11.2134.
11. Rahman MN, Othman NFB. A numerical model for ash deposition based on actual operating conditions of a 700 MW coal-fired power plant: Validation feedback loop via structural similarity indexes (SSIMs). CFD Lett. 2022;14(1):99. https://doi.org/10.37934/cfdl.14.1.99111.
12. Rahman MN, MS Aris, MH Ujir, MH Boosroh, Pillai DPV. Predictive numerical analysis to optimize ventilation performance in a hydropower surge chamber for H_2S removal. CFD Lett. 2021; 13(10): 69. https://doi.org/10.37934/cfdl.13.10.6980
13. Tarrazo E, Sánchez AL, Liñán A, Williams FA. A simple one-step chemistry model for partially premixed hydrocarbon combustion. Combust Flame. 2006. https://doi.org/10.1016/j.combustflame.2006.08.001.
14. Carbajal-Carrasco LA, Bouali Z, Mura A. Optimized single-step (OSS) chemistry for auto-ignition of heterogeneous mixtures. Combust Flame. 2021. https://doi.org/10.1016/j.combustflame.2020.12.026.
15. Yao S, Tang X, Luan M, Wang J. Numerical study of hollow rotating detonation engine with different fuel injection area ratios. Proc Combust Inst. 2017. https://doi.org/10.1016/j.proci.2016.07.126.
16. Jin S, Qi L, Zhao N, Zheng N, Meng Q, Yang J. Experimental and numerical research on rotating detonation combustor under non-premixed conditions. Int J Hydrog Energy. 2020. https://doi.org/10.1016/j.ijhydene.2020.02.009.
17. Xiao H, Oran ES. Shock focusing and detonation initiation at a flame front. Combust Flame. 2019. https://doi.org/10.1016/j.combustflame.2019.02.012.
18. Xia Z, Tang X, Luan M, Zhang S, Ma Z, Wang J. Numerical investigation of two-wave collision and wave structure evolution of rotating detonation engine with hollow combustor. Int J Hydrog Energy. 2018. https://doi.org/10.1016/j.ijhydene.2018.09.165.
19. Tang XM, Wang JP, Shao YT. Three-dimensional numerical investigations of the rotating detonation engine with a hollow combustor. Combust Flame. 2015. https://doi.org/10.1016/j.combustflame.2014.09.023.
20. Katta VR, Cho KY, Hoke JL, Codoni JR, Schauer FR, Roquemore WM. Effect of increasing channel width on the structure of rotating detonation wave. Proc Combust Inst. 2019. https://doi.org/10.1016/j.proci.2018.05.072.
21. Meng Q, Zhao N, Zheng H, Yang J, Qi L. Numerical investigation of the effect of inlet mass flow rates on H_2/air non-premixed rotating detonation wave. Int J Hydrog Energy. 2018. https://doi.org/10.1016/j.ijhydene.2021.10.270.
22. Yao S, Ma Z, Zhang S, Luan M, Wang J. Reinitiation phenomenon in hydrogen-air rotating detonation engine. Int J Hydrog Energy. 2017. https://doi.org/10.1016/j.ijhydene.2017.09.015.
23. Yao S, Wang J. Multiple ignitions and the stability of rotating detonation waves. Appl Therm Eng. 2016. https://doi.org/10.1016/j.applthermaleng.2016.07.166.
24. Frolov SM, Dubrovskii AV, Ivanov VS. Three-dimensional numerical simulation of the operation of a rotating-detonation chamber with separate supply of fuel and oxidizer. Russ J Phys Chem B. 2013. https://doi.org/10.1134/S1990793112010071.
25. Liu M, Zhou R, Wang JP. Numerical investigation of different injection patterns in rotating detonation engines. Combust Sci Technol. 2014. https://doi.org/10.1080/00102202.2014.923411.

26. Sun J, Zhou J, Liu S, Lin Z, Lin W. Plume flowfield and propulsive performance analysis of a rotating detonation engine. Aerosp Sci Technol. 2018. https://doi.org/10.1016/j.ast.2018.08.024.
27. Rahman MN, Wahid MA. Renewable-based zero-carbon fuels for the use of power generation: A case study in Malaysia supported by updated developments worldwide. Energy Rep. 2021. https://doi.org/10.1016/j.egyr.2021.04.005.
28. Feroskhan M, Ismail S, Panchal SH. Study of methane enrichment in a biogas fuelled HCCI engine. Int J Hydrog Energy. 2021. https://doi.org/10.1016/j.ijhydene.2021.02.216.
29. Huang Y, Xia H, Chen X, Luan Z, You Y. Shock dynamics and expansion characteristics of an aerospike nozzle and its interaction with the rotating detonation combustor. Aerosp Sci Technol. 2021. https://doi.org/10.1016/j.ast.2021.106969.
30. Sun J, Zhou J, Liu S, Lin Z, Lin W. Effects of air injection throat width on a non-premixed rotating detonation engine. Acta Astronaut. 2019. https://doi.org/10.1016/j.actaastro.2019.03.067.
31. Menter FR. Two-equation eddy-viscosity turbulence models for engineering applications. AIAA J. 1994. https://doi.org/10.2514/3.12149.
32. Menter FR. Review of the shear-stress transport turbulence model experience from an industrial perspective. Int J Comput Fluid Dyn. 2009. https://doi.org/10.1080/10618560902773387.
33. Zheng H, Meng Q, Zhao Q, Li Z, Deng F. Numerical investigation on H_2/Air non-premixed rotating detonation engine under different equivalence ratios. Int J Hydrog Energy. 2020. https://doi.org/10.1016/j.ijhydene.2019.11.014.
34. Ganju S, Karanam A, Mishra S, Saha N, Gera B, Goyal P, Sharma PK, Shelke AV. 7 - Application of CFD for assessment of containment safety. Adv Comput Fluid Dyn Nucl React Design Saf Assess. 2019. https://doi.org/10.1016/B978-0-08-102337-2.00007-9.
35. Xia Z, Ma H, Liu C, Zhuo C, Zhou C. Experimental investigation on the propagation mode of rotating detonation wave in plane-radial combustor. Exp Therm Fluid Sci. 2019. https://doi.org/10.1016/j.expthermflusci.2019.01.032.
36. Zheng K, Xufeng Y, Yu M, Si R, Wang L. Effect of N_2 and CO_2 on explosion behavior of syngas/air mixtures in a closed duct. Int J Hydrog Energy. 2019. https://doi.org/10.1016/j.ijhydene.2019.09.053.
37. Westbrook CK, Dryer FL. Simplified reaction mechanisms for the oxidation of hydrocarbon fuels in flames. Combust Sci Techno. 1981. https://doi.org/10.1080/00102208108946970.
38. Silva VB, João C. Computational fluid dynamics applied to waste-to-energy processes: a hands-on approach. Butterworth-Heinemann; 2020
39. Coates AM, Mathias DL, Cantwell BJ. Numerical investigation of the effect of obstacle shape on deflagration to detonation transition in a hydrogen–air mixture. Combust Flame. 2019. https://doi.org/10.1016/j.combustflame.2019.07.044.
40. Rakotoarison W, Maxwell B, Pekalski A, Radulescu MI. Mechanism of flame acceleration and detonation transition from the interaction of a supersonic turbulent flame with an obstruction: Experiments in low pressure propane–oxygen mixtures. Proc Combust Inst. 2019. https://doi.org/10.1016/j.proci.2018.08.050.
41. Zheng W, Kaplan C, Houim R, Oran E. Flame acceleration and transition to detonation: Effects of a composition gradient in a mixture of methane and air. Proc Combust Inst. 2019. https://doi.org/10.1016/j.proci.2018.07.118.
42. Wei S, Yu M, Pei B, Zhu Z, Zhang Z. Suppression of CO_2 and H_2O on the cellular instability of premixed methane/air flame. Fuel. 2020. https://doi.org/10.1016/j.fuel.2019.116862.
43. Fischer M, Jiang M. An investigation of the chemical kinetics of biogas combustion. Fuel. 2015. https://doi.org/10.1016/j.fuel.2015.01.085.
44. Li Q, Liu P, Zhang H. Further investigations on the interface instability between fresh injections and burnt products in 2-D rotating detonation. Comput Fluids. 2018. https://doi.org/10.1016/j.compfluid.2018.05.005.
45. Driscoll R, St. George A, Gutmark EJ. Numerical investigation of injection within an axisymmetric rotating detonation engine. Int J Hydrog Energy. 2016; 41(3): 2502 https://doi.org/10.1016/j.ijhydene.2015.10.055
46. Radulescu MI, Hanson RK. Effect of heat loss on pulse-detonation-engine flow fields and performance. J Propul Power. 2005. https://doi.org/10.2514/1.10286.
47. Ishii K, Itoh K, Tsuboi T. A study on velocity deficits of detonation waves in narrow gaps. Proc Combust Inst. 2002. https://doi.org/10.1016/S1540-7489(02)80340-6.
48. Huang J, Han W, Gao X, Wang C. Effects of heat loss and viscosity friction at walls on flame acceleration and deflagration to detonation transition. Chin Phys B. 2019. https://doi.org/10.1088/1674-1056/28/7/074704.
49. Gordon S, McBride BJ. Computer program for calculation complex chemical equilibrium compositions and applications (I. Analysis). NASA Reference publication 1311. 1994. https://ntrs.nasa.gov/citations/19950013764
50. Wang C, Qian C, Liu J, Liberman MA. Influence of chemical kinetics on detonation initiating by temperature gradients in methane/air. Combust Flame. 2018. https://doi.org/10.1016/j.combustflame.2018.08.017.
51. Dounia O, Vermorel O, Misdariis A, Poinsot T. Influence of kinetics on DDT simulations. Combust Flame. 2019. https://doi.org/10.1016/j.combustflame.2018.11.009.
52. Marco A, Shepherd JE. A numerical study of detonation diffraction. J Fluid Mech. 2005. https://doi.org/10.1017/S0022112005003319.